JURNAL SAINS MATERI INDONESIA (JUSAMI)
ISSN: 1411-1098 (print), 2614-087X (online)
VOL. 27, ISSUE 1, 2026
DOI: https://doi.org/10.55981/jsmi.2026.13450

ORIGINAL ARTICLE

Characteristics and Photocatalytic Performance of Coprecipitation Praseodymium (Pr)-doped Strontium Titanate for Methylene Blue Degradation

S. N. Khoiria[1], D. K. Sandi[2], F. Nurosyid[1], R. Suryana[1], Y. Iriani[1*]

[1]Department of Physics, Faculty of Mathematics and Natural Sciences, Universitas Sebelas Maret, Indonesia
[2]Study Program of Energy Conversion Engineering, Department of Mechanical Engineering, Semarang State Polytechnic, Indonesia

ABSTRACT – Strontium titanate ($SrTiO_3$ or STO) is a perovskite material with promising photocatalytic properties for wastewater degradation. Doping with rare-earth elements such as praseodymium (Pr) can enhance its performance by modifying structural and electronic characteristics. In this study, Pr-doped STO ($Sr_{1-x}Pr_xTiO_3$, x = 0%, 2%, and 4%) was synthesized via the coprecipitation method. X-ray diffraction (XRD) confirmed a single-phase perovskite structure with high crystallinity, while Fourier transform infra-red (FTIR) analysis verified the formation of Sr–Ti–O bonds. Particle size analysis (PSA) and surface area analysis (SAA) with the Brunauer-Emmett-Teller (BET) method revealed that higher Pr concentrations reduced particle size and increased surface area. Photocatalytic activity was evaluated using methylene blue (MB) degradation under ultraviolet (UV) irradiation for up to 5 hours. The $Sr_{0.98}Pr_{0.02}TiO_3$ sample exhibited the best performance, achieving 73.08% MB degradation after 5 hours, demonstrating the effectiveness of moderate Pr doping in enhancing photocatalytic activity.

ARTICLE HISTORY
Received: 11 Aug 2025
Revised: 21 Sep 2025
Accepted: 24 Okt 2025

KEYWORDS
Strontium titanate
Praseodymium doping
Photocatalyst
MB dye
Photodegradation

INTRODUCTION

The textile industry is a major contributor to environmental pollution, primarily due to the use of synthetic dyes such as methylene blue (MB). These dyes are stable, difficult to biodegrade, and accumulate in aquatic ecosystems, posing serious environmental and health risks [1]–[3]. Therefore, effective wastewater treatment methods are needed to address this problem.

Photodegradation has been widely studied as a promising technique for wastewater treatment [2], [4], [5]. It can mineralize hazardous organic pollutants into non-toxic products such as carbon dioxide (CO_2) and water (H_2O) without generating secondary waste [3], [4]. Various semiconductor materials have been developed for this application, one of which is strontium titanate ($SrTiO_3$ or STO), known for its high thermal stability, environmental friendliness, and potential as a photocatalyst [6], [7]. However, pure STO is only active in the ultraviolet (UV) region due to its relatively wide bandgap of approximately 3.20 eV, severely limiting its use in visible light [8], [9].

To overcome this limitation, several modification strategies have been proposed, including metal/non-metal doping, surface modification, and heterostructure formation. Among these, rare earth ion doping is an attractive approach because it can change the energy band structure, form intermediate energy levels, and improve the efficiency of electron-hole pair analysis [10]–[12]. Song et al. have demonstrated doping STO with various rare-earth ions (Y^{3+}, La^{3+}, Ce^{3+}, Pr^{3+}, Nd^{3+}, Sm^{3+}, Eu^{3+}, Gd^{3+}, Tb^{3+}, Dy^{3+}, Ho^{3+}, Er^{3+}, Tm^{3+}, Yb^{3+}, and Lu^{3+}), with Gd-doped STO showing the highest efficiency (~99%), while dysprosium (Dy) doping exhibited the lowest performance [12]. Besides, a perovskite-based material, $Sr_2La_{0.5}R_{0.5}FeMnO_7$ (R = Nd, Sm, Gd, Dy), achieved 97–99% MB degradation efficiency in just 50 minutes, with gadolinium (Gd) doping showing the best results [10]. Furthermore, a $CeO_2/SrTiO_3$ heterojunction-based photocatalyst reached nearly 100% degradation in 40 minutes due to efficient radical generation and porous structure[13].

Beyond STO, praseodymium (Pr) doping has shown promising effects in other oxide systems. For example, Pr-doped titanium dioxide (TiO_2) improved crystallinity, light absorption, and dye conversion [14], [15]. Fe–Pr co-doping on TiO_2 decreased the band gap and increased the number of oxygen vacancies, thereby synergistically enhancing the photocatalytic activity [16]. Pr-doped ZnO nanoparticles have been proven to enhance methyl orange and organic pollutants degradation due to less electron-hole recombination and improved optical response [17], [18]. These findings suggest that Pr is a promising dopant for improving the photocatalytic performance of semiconductors.

Despite these advances, research on Pr-doped $SrTiO_3$ remains very limited compared to other rare-earth dopants such as La, Nd, Ce, and Gd. Moreover, most existing studies employed sol–gel or solid-state methods, which are energy-intensive,

*CORRESPONDING AUTHOR | S. N. Khoiria | ✉ salsanurulkhoiria@student.uns.ac.id

complex, and less scalable. In contrast, the coprecipitation method offers a simpler, cost-effective, and environmentally friendly approach capable of producing highly homogeneous particles with controlled sizes [9], [19]. However, reports on Pr-doped $SrTiO_3$ synthesized via coprecipitation are still scarce. Furthermore, the relationship between Pr concentration, structural and morphological modification, and photocatalytic efficiency in MB degradation under visible light remains insufficiently understood.

Based on these gaps, this study aimed to synthesize $Sr_{1-x}Pr_xTiO_3$ (x = 0; 0.02; 0.04) via the coprecipitation method and to investigate the influence of Pr doping on the crystal structure, morphological, optical properties, and photocatalytic activity in MB degradation. The outcomes are expected to provide new insights into the role of Pr in tailoring the photocatalytic performance of $SrTiO_3$. Besides, the results are expected to demonstrate coprecipitation as a feasible method for producing efficient and eco-friendly photocatalysts for textile wastewater treatment.

EXPERIMENTAL METHOD

Preparation of $Sr_{1-x}Pr_xTiO_3$

The synthesis of $Sr_{1-x}Pr_xTiO_3$ (x was the praseodymium (Pr) mole concentrations: 0, 2%, 4%) was carried out using the coprecipitation method. The chemicals used included strontium nitrate [$Sr(\sim NO_3)_2$] (Sigma-Aldrich, ≥ 99%), titanium(IV) butoxide [$Ti(C_4H_9O)_4$] (Sigma-Aldrich, 97%), oxalic acid [$C_2H_2O_4$] (Sigma-Aldrich, ≥ 99%), and praseodymium(III) acetate hydrate [$Pr(OOCCH_3)_3 \cdot H_2O$] (Alfa Aesar, 99.9%) and 2-propanol [$(CH_3)_2CHOH$] (Sigma-Aldrich, ≥ 99%).

$C_2H_2O_4$ was dissolved in isopropanol (IPA) and stirred using a hotplate stirrer for 20 minutes at 250 rpm to form solution A. Individually, $Ti(C_4H_9O)_4$ solution was mixed with IPA, and the mixture was added to Solution A and stirred for 20 minutes at the same speed. Next, $Sr(NO_3)_2$ and the doping agent [$Pr(OOCCH_3)_3 \cdot H_2O$] were added simultaneously to the mixture and stirred for 30 minutes until the solution was homogeneous. The titration process was carried out by slowly adding distilled water while stirring continuously at 250 rpm, and then left for 24 hours to obtain the precipitates. They were washed three times with ethanol and distilled water until they reached a neutral pH.

The precipitates were then hydrolyzed by heating in an oven at 100 °C for 10 hours until all the water was removed. The resulting powders were ground until homogeneous. Next, the sample powders were sintered at 1000 °C for 4 hours. The final samples were ground for 30 minutes to obtain a more homogeneous powder.

Material Characterization

Bruker D8 Advanced X-ray Diffraction (XRD) was used to identify the crystal structure, lattice parameters, and crystallinity of the samples. Crystalline size analysis was performed using the Debye–Scherrer method, as Equation (1) [9].

$$D = \frac{K\lambda}{\beta \cos\theta} \tag{1}$$

Shimadzu (serial number A21004802518) Fourier transform infra-red (FTIR) spectroscopy was employed to identify functional groups of the samples in the wave number range 350 cm^{-1}–4000 cm^{-1}. Quantachrom (version 10.01) surface area analyzer (SAA) was performed to examine the Brunauer-Emmett-Teller (BET) specific surface area of the samples using N_2 adsorption-desorption. Malvern Panalytical Zetasizer (Ver. 8.00.4813) particle size analyzer (PSA) was employed to determine particle size distribution and the polydispersity index (PDI) value as an indicator of particle size homogeneity. PECORD 200 PLUS-223E1117F UV-Vis reflectance diffuse spectroscopy (UV-Vis DRS) was utilized to investigate the absorption spectra of the samples. The data were then exploited to estimate the band gap energy value using the Tauc–Kubelka–Munk method, as Equation (2). The band gap energy was obtained by extrapolating the Tauc plot, a graph of $(F(R_\infty)hv)^{\frac{1}{n}}$ against energy (hv) [20], [21].

$$(F(R_\infty)hv)^{\frac{1}{n}} = C(hv - E_g) \tag{2}$$

Photocatalytic Test

The photocatalytic activity of pure and Pr-doped strontium titanate ($SrTiO_3$ or STO) samples was examined against methylene blue (MB). Prior to this, 10 mg of MB powder was dissolved in 1000 mL of distilled water, producing a 10 ppm MB solution. For the photocatalytic examination, every 10 mg of the prepared photocatalysts was dissolved in 10 mL of the MB solution. The mixtures were then stirred in a dark condition for 30 min to reach an equilibrium condition. After that, they were exposed to a ultraviolet (UV) lamp for various periods of 0, 1, 2, 3, 4, and 5 hours. The exposed solutions were taken at the specific times, and the absorbances were measured using a HITACHI UH5300 UV-Vis spectrophotometer in the wavelength range of 400–800 nm. The absorbance data were then utilized to compute the MB degradation level through Equation (3). In this equation, A_0 and A_t are the absorbances before and after UV exposure at the specified t periods, respectively [3], [19].

$$MB\ degradation\ level = \left(\frac{A_0 - A_t}{A_0}\right) \times 100\% \tag{3}$$

RESULT AND DISCUSSION

The diffractograms of the pristine and Pr-doped strontium titanate ($SrTiO_3$ or STO) samples are shown in Figure 1. All the main peaks can be indexed and are in accordance with the ICDD database number #84-0444. This confirms that all prepared materials possess a cubic perovskite crystal structure with the space group *Pm3m*, corresponding to the STO system. In addition, additional peaks (marked with * and • symbols) were detected, indicating the formation of secondary phases in the form of $SrCO_3$ and TiO_2, according to the ICDD database No. #84-1778 and #86-0147, respectively. The presence of $SrCO_3$ can be related to the interaction of the synthesized SrO_3 with CO_2 during the reaction process. Meanwhile, TiO_2 was formed due to the tendency of Ti^{4+} ions to undergo hydrolysis under humid conditions, thus crystallizing as the TiO_2 phase.

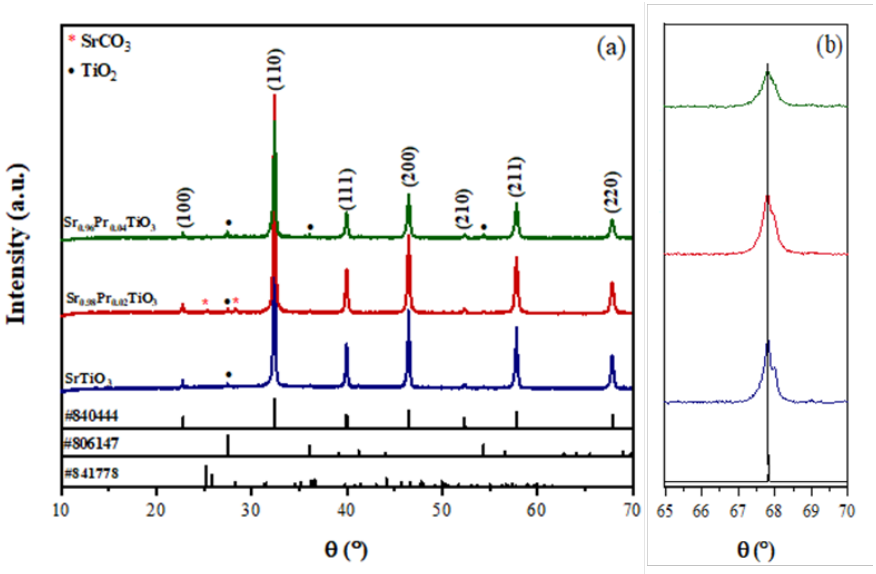

Figure 1. (a) Diffractograms of pure and Pr-doped STO samples corresponding to the $SrTiO_3$ system based ICDD database, and (b) the peaks magnification at (220) planes showing a shift due to Pr doping

Table 1. Calculated lattice constant, crystallite size, and crystallinity of pure and Pr-doped STO

Samples	Crystallinity (%)	Crystallite size (nm)	Lattice constants a=b=c (nm)
$SrTiO_3$	50.77	37.55	0.39069
$Sr_{0.98}Pr_{0.02}TiO_3$	57.42	31.04	0.39067
$Sr_{0.96}Pr_{0.04}TiO_3$	51.57	28.59	0.39066

Peak shift analysis (Figure 1(b)), particularly on the (220) plane, shows a shifted peak to a smaller 2θ angle, indicating a decrease in crystallite size due to Pr doping [16]. Table 1 summarizes the crystallite size, lattice parameter, and crystallinity of the samples. The undoped $SrTiO_3$ has a crystallite size of 37.55 nm with a lattice parameter of 0.39069 nm and a crystallinity of 50.77%. After Pr doping, the crystallite size decreases to 31.04 nm (Pr 2%) and 28.59 nm (Pr 4%), accompanied by a gradual decrease in the lattice parameter. This phenomenon can be explained by the difference in ionic radii between Sr^{2+} (1.18 Å) and Pr^{3+} (0.99 Å), where substitution of Sr^{2+} by Pr^{3+} causes shrinkage of the crystal lattice [21]. Furthermore, the crystallinity level increased at 2% doping (57.42%) and slightly decreased at 4% doping (51.57%). This indicates that moderate Pr doping can improve structural order, but excessive doping tends to introduce crystal defects that decrease crystallinity [22], [23]. These findings demonstrate that Pr doping successfully interacts within the $SrTiO_3$ lattice, characterized by changes in crystal size, shrinkage of the lattice parameter, and variations in crystallinity, although secondary $SrCO_3$ and TiO_2 phases are still present in the sample.

The Fourier transform infra-red (FTIR) spectra of pure and Pr-doped STO samples are shown in Figure 2. In general, all samples exhibit the main absorption bands typical of $SrTiO_3$. Differences in Pr doping concentrations cause an insignificant slight wavenumber shift within the observed functional group range [18]. The strong absorption band located in 570.95–575.78 cm^{-1} was associated with the vibrations of the Sr–Ti–O bond in the perovskite structure [19]. The intensity of this band tends to decrease with increasing Pr doping concentration, indicating lattice distortion due to the substitution of Sr^{2+} by Pr^{3+}. This is consistent with the results of X-ray diffraction (XRD) analysis, which showed changes in the lattice parameter and crystallite size. In addition, several other absorption bands were also identified at bands of 1514.19–1516.11 cm^{-1}, 2313.71–2314.16 cm^{-1}, and 3423.76 cm^{-1}, corresponding to C–H, C–O–O, and O–H stretching vibrations, respectively [20]–[22]. The presence of these bands generally originates from residual organic contaminants, carbonates, or water molecules

adsorbed on the sample surface during the synthesis and storage process. The yields confirm the XRD findings that Pr doping successfully affects the local structure of $SrTiO_3$.

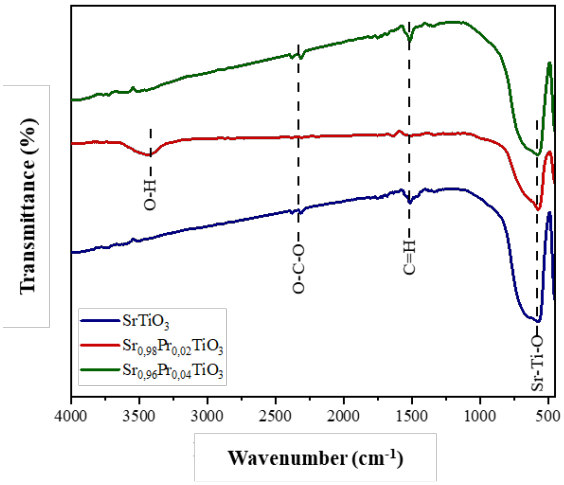

Figure 2. FTIR spectra of pristine and Pr-doped $SrTiO_3$ exhibiting the main absorption bands typical of $SrTiO_3$ and an insignificant slight shift in wavenumber due to different Pr doping concentrations

The morphological surfaces of all samples with varying Pr mole concentrations are presented in Figure 3. Pure STO exhibits a relatively even particle agglomeration, with grain sizes ranging from nanometers to sub-micrometres. The surface structure appears dense, with small pores scattered among the agglomerates. With the addition of 2% Pr doping, the surface morphology reveals increased agglomeration and a more diverse grain size distribution. At Pr 4% doping ($Sr_{0.96}Pr_{0.04}TiO_3$), particle agglomeration becomes more pronounced, with grains appearing larger and denser than those in $Sr_{0.98}Pr_{0.02}TiO_3$ and pure STO. This indicates that the addition of Pr dopant at higher concentrations can accelerate grain growth, potentially affecting the specific surface area of the samples [15], [22], [24]. In general, scanning electron microscopy (SEM) results confirm that Pr doping affects the surface morphology of $SrTiO_3$[3], particularly in terms of particle size distribution and degree of agglomeration. These changes align with the structural and functional group analyses, which indicate lattice distortion due to the substitution of Sr^{2+} by Pr^{3+} [20], [25], [26].

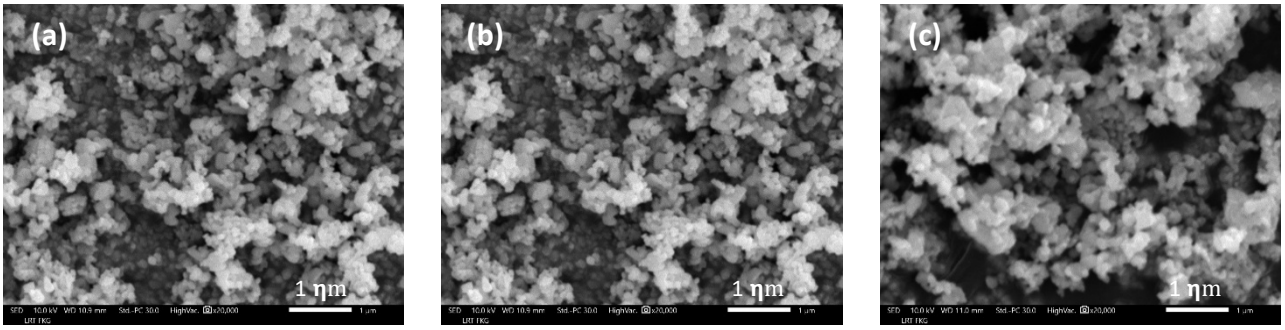

Figure 3. Morphological images of (a) pristine STO, (b) $Sr_{0.98}Pr_{0.02}TiO_3$, and (c) $Sr_{0.6}Pr_{0.04}TiO_3$. The images demonstrate agglomeration and grain growth affected by different Pr doping concentrations.

Average particle sizes, polydispersity index (PDI) indexes, and Brunauer-Emmett-Teller (BET) specific surface area of pristine and Pr-doped STO are presented in Table 2. The average particle size of the pure STO was 331.6 nm with a PDI value of 0.233, indicating a relatively narrow particle distribution. At 2% Pr doping, the average particle size increased to 375.1 nm with a higher PDI (0.440), denoting a wider particle size distribution due to agglomeration [27], [28]. Conversely, at 4% Pr doping, the average particle size decreased to 285.7 nm with a PDI of 0.197, representing a more uniform distribution [28]. Although not a Pr-doped sample, a similar study also reported that the dopant addition could affect polydispersity and agglomeration, especially increasing particle size & PDI values [29].

Table 2. Average particle sizes, PDI, and BET specific surface area of pristine and Pr-doped STO

Samples	Average particle sizes (nm)	PDI	BET specific surface area (m^2/g)
$SrTiO_3$	331.6	0.233	3.914
$Sr_{0.98}Pr_{0.02}TiO_3$	375.1	0.440	6.447
$Sr_{0.96}Pr_{0.04}TiO_3$	285.7	0.197	5.291

Additionally, pristine STO had a surface area of 3.914 m²/g, while $Sr_{0.98}Pr_{0.02}TiO_3$ produced the highest value of 6.447 m²/g. This can be attributed to increased agglomeration and particle size heterogeneity at this concentration [30]. The maximum surface area observed in $Sr_{0.98}Pr_{0.02}TiO_3$ is consistent with literature reports that rare earth substitution in $SrTiO_3$ can alter the local structure and particle growth, resulting in non-monotonic changes in particle size and surface area depending on the synthesis conditions; the increase in PDI and broader size distribution at low doping are generally associated with agglomeration and hence with changes in the measured BET values [31]. The surface area of $Sr_{0.96}Pr_{0.04}TiO_3$ declined to 5.291 m²/g, likely due to the growth of larger grains, as observed in the morphological feature (Figure 3 (c)). Overall, these results indicate that variations in Pr concentration influence the particle size, distribution, and surface area of the material [31]–[33]. The largest surface area at $Sr_{0.98}Pr_{0.02}TiO_3$ has the potential to provide more active sites for surface reactions, beneficial in photocatalytic applications.

The band gap values of pure and Pr-doped STO samples, obtained from the Tauc plots in Figure 4, showed a decrease from 3.16 eV for pure STO to 3.13 eV for $Sr_{0.98}Pr_{0.02}TiO_3$ and 3.10 eV for $Sr_{0.96}Pr_{0.04}TiO_3$. This decrease indicates that the substitution of Pr^{3+} ions on Sr^{2+} sites changes the electronic structure of $SrTiO_3$, resulting in a narrower band gap. Similar trends have been reported in theoretical and experimental studies, which confirm that rare earth (RE) doping, especially with Pr, introduces energy levels within the band gap, reduces the band gap energy, and enhances visible light absorption [20], [34], [35].

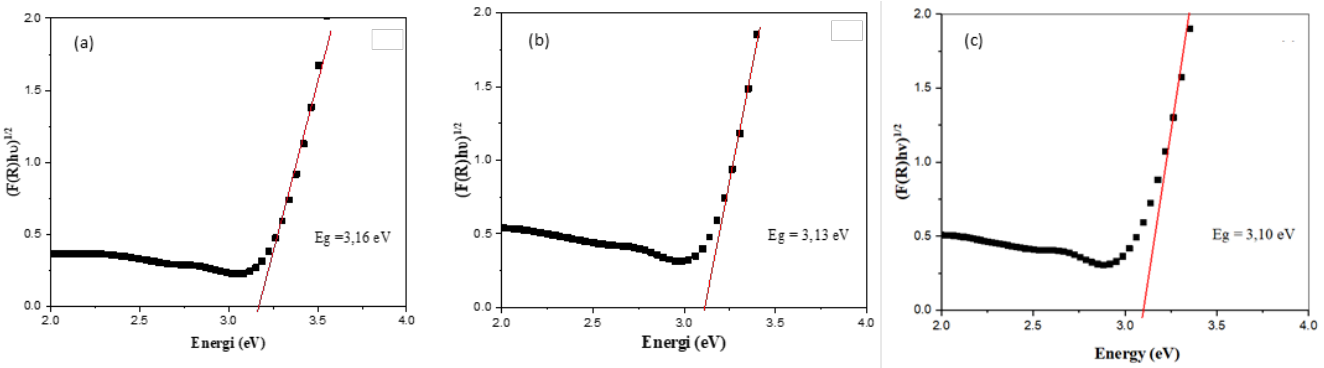

Figure 4. Tauc Plots for band gap estimations: (a) $SrTiO_3$, (b) $Sr_{0.98}Pr_{0.02}TiO_3$, and (c) $Sr_{0.96}Pr_{0.04}TiO_3$, shows the bandgap energy values declined due to Pr doping

The band gap narrowing in Pr-doped $SrTiO_3$ is due to Pr^{3+} substitution at Sr^{2+} sites, as confirmed by lattice shrinkage and peak shifts in XRD, as reported in [23]. This heterovalent substitution induces oxygen vacancies and defect states near the band edges, narrowing the bandgap [36]–[38]. Although higher Pr content (x = 4%) causes increased agglomeration and compaction of the grains, quantum confinement effects can be ruled out because the particle size remained in the hundreds of nanometers, leaving surface irregularities and defects as the dominant factors [21], [39], [40]. Particle size analysis (PSA) results showed reduced particle size and improved uniformity at x = 4%, while surface area analysis (SAA) exhibited the highest surface area at x = 2%. Nonetheless, the lowest band gap occurred at x = 4%, highlighting that electronic structure modification from Pr doping, rather than surface area, plays a major role, with minor secondary phases contributing insignificantly [40], [41].

The methylene blue (MB) degradation absorbance spectra of pure and Pr-doped STO samples at different irradiation times are shown in Figure 5(a), Figure 5(b), and Figure 5(c). The decrease in MB peak intensity indicates continuous degradation, further supported by the calculated degradation percentage (Figure 5(d)). Among these samples, $Sr_{0.98}Pr_{0.02}TiO_3$ exhibited the highest photocatalytic efficiency, reaching 73.08% degradation after 5 hours of irradiation. Kinetic analysis (Figure 5(e) and Figure 5(f)) showed that this sample also had the highest reaction rate constant ($k = 0.2151\ min^{-1}$), while higher doping (4% Pr) resulted in decreased photocatalytic activity.

These results are consistent with the structural and optical characterization. XRD confirmed that all samples retained a perovskite structure. At the same time, Pr doping induced slight variations in lattice parameters and crystallite size, which promoted the formation of defects that facilitate electron-hole separation [41]. SEM analysis revealed a more uniform

morphology for the 2% doped sample. In contrast, PSA and SAA measurements revealed the largest specific surface area at this doping level, which offers more active sites for dye interaction [42]–[44]. Furthermore, UV-Visible analysis confirmed that Pr doping narrowed the band gap, enhancing light absorption and charge generation [45]–[47]. Collectively, the superior performance of $Sr_{0.98}Pr_{0.02}TiO_3$ arises from the synergy of structural stability, favorable morphology, larger surface area, and optimized band gap, which enables efficient charge transfer [47]. Contrarily, excessive doping (4% Pr) introduces surplus defects and recombination centres, reduces the effective surface area, and alters the morphology, ultimately suppressing the photocatalytic activity [43], [48].

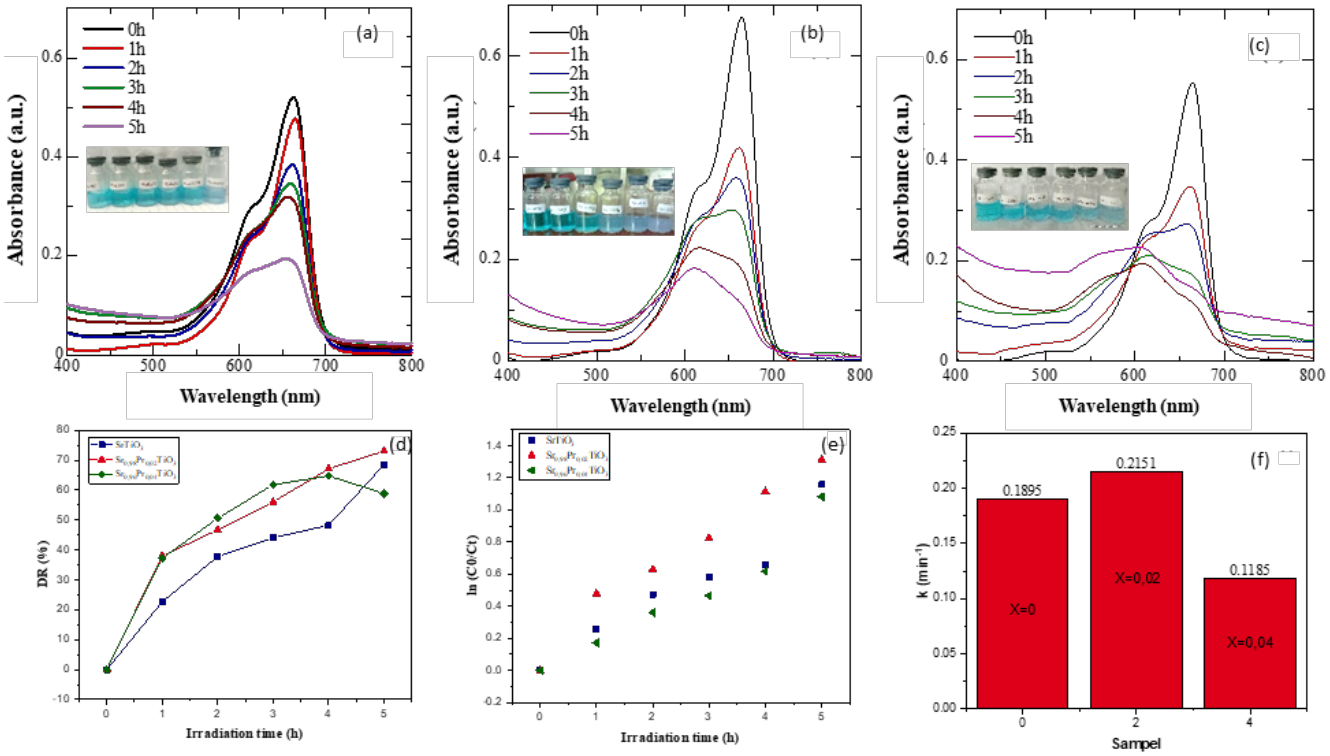

Figure 5. Absorbance curves of degraded MB solution by (a) $SrTiO_3$, (b) $Sr_{0.98}Pr_{0.02}TiO_3$, and (c) $Sr_{0.96}Pr_{0.04}TiO_3$, (d) MB degradation levels by pristine and Pr-doped STO corresponding to exposure times, (e) MB degradation kinetics by all prepared photocatalysts, and (f) kinetic rates of MB degradation for pristine and Pr-doped STO samples

Based on the structural and optical analyses, the improvement in photocatalytic activity can be explained by a mechanism mediated by defects induced by Pr. Substitution of Sr^{2+} with Pr^{3+} introduces lattice distortions and oxygen vacancies, which act as shallow traps that delay electron–hole recombination. Under UV illumination, electrons are excited from the valence band (VB) to the conduction band (CB), leaving holes in the VB. The presence of Pr-related defect states helps charge separation, allowing electrons to reduce O_2 into $\bullet O_2^-$ radicals, while holes oxidize H_2O to •OH radicals. These species are primarily responsible for MB degradation. A schematic band diagram illustrating this mechanism is provided in Figure 6.

Meanwhile, for the detected minor phases of $SrCO_3$ and TiO_2, although these secondary phases are not dominant, they may still affect the photocatalytic activity. For example, TiO_2 can act as an additional photocatalyst under UV illumination, potentially contributing to dye degradation [49]. However, the relatively low peak intensity of TiO_2 indicates its limited contribution compared to the overall $SrTiO_3$ matrix. On the other hand, $SrCO_3$ is generally not photocatalytically active and may act as an impurity rather than an active phase [50], [51]. Thus, these secondary phases may have a slight effect and can be negligible. The performance improvement is mainly due to the incorporation of Pr into the $SrTiO_3$ lattice.

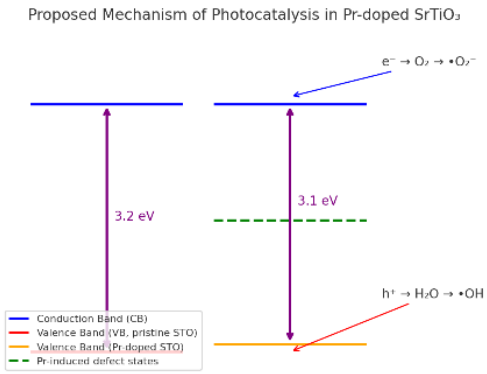

Figure 6. Energy band diagram showing how Pr doping facilitates charge separation and reduces recombination in Pr-doped $SrTiO_3$

To reinforce the novelty of this study, comparisons with prior Pr-doped studies on other oxides are summarized. On Pr-doped TiO_2, Doğu & Gürkan [14] reported increased MB degradation efficiency depending on the dopant ratio and thermal conditions. They recorded an increased efficiency in TiO_2 by ~25–40% compared to pure TiO_2 under comparable conditions. On Pr-doped ZnO, Ahmad et al. [17] reported an improvement in the decomposition of organic pollutants with significantly increased reaction rates. This comparison indicates that Pr is generally effective in oxide semiconductor systems due to its ability to introduce low-energy levels and modulate oxygen concentration.

However, the performance of $Sr_{0.98}Pr_{0.02}TiO_3$ demonstrated here was still lower than that of several other rare dopants on STO. For example, Song et al. [12] reported that Gd-doped $SrTiO_3$ achieved almost complete methylene blue degradation (~99%) within 5 h. Meanwhile, La-doped $SrTiO_3$ by Iriani et al. [19] could reach approximately 85% under similar UV irradiation. Ce-based modifications, such as the $CeO_2/SrTiO_3$ heterojunction, have been shown to degrade nearly 100% of MB in only 40 min. [13].

Although its efficiency was lower than that of gadolinium (Gd) or cerium (Ce) -doped systems, the result remains significant by offering two main contributions. First, it presents the first quantitative benchmark for Pr-doped $SrTiO_3$ synthesized via coprecipitation, demonstrating that Pr addition could effectively reduce the band gap, increase the surface area, and enhance activity compared to pure $SrTiO_3$. Second, it shows that although Pr improves the performance compared to pure $SrTiO_3$, to achieve equivalent efficiency to Gd/Ce, further optimization, such as co-doping, heterojunction formation, or secondary phase control, is required.

The kinetic constant obtained for $Sr_{0.98}Pr_{0.02}TiO_3$ is also comparable with values reported for the other rare-earth-doped $SrTiO_3$ systems. For instance, La-doped $SrTiO_3$ prepared via coprecipitation achieved a rate constant of ~0.19 min^{-1} under UV irradiation [19], while Gd-doped $SrTiO_3$ exhibited higher values around 0.28–0.32 min^{-1} depending on the synthesis method [12]. In addition, Pr-doped TiO_2 and ZnO systems typically show rate constants in the range of 0.18–0.25 min^{-1} [14], [17]. These comparisons confirm that the kinetics observed in this study align with previous findings, validating that Pr incorporation effectively enhances the degradation rate relative to pristine $SrTiO_3$.

Lastly, it is important to emphasize that the photocatalytic tests in this study were performed under UV irradiation. In this study, UV was deliberately chosen to allow direct comparison with previously reported doped $SrTiO_3$ systems and establish a controlled proof-of-concept of the effect of Pr doping before exploring more complex visible-light modifications. Therefore, the enhanced activity observed here arises primarily from improved charge separation and surface reactivity under UV light rather than visible-light activation. This distinction is crucial, as many $SrTiO_3$-based systems require further modification (e.g., co-doping or heterojunction formation) to achieve efficient visible-light response. Hence, the implication for practical wastewater treatment is that although Pr doping alone cannot make $SrTiO_3$ a visible-light catalyst, Pr doping can serve as a basis for further strategies (e.g., coupling with narrow-bandgap semiconductors, co-doping, or constructing heterostructures) to extend the absorption into the visible region.

CONCLUSION

This study successfully synthesized pure and Pr-doped STO (2% and 4%) via the coprecipitation method and investigated the effect of Pr doping on their structural, morphological, optical, and photocatalytic properties. Moderate doping (x = 2%) achieved the best balance between lattice distortion, morphology, surface area, and band gap narrowing, resulting in the highest MB degradation efficiency, while excessive doping (x = 4%) decreased the activity due to defect-induced recombination. These findings highlight the importance of optimizing the Pr concentration, with 2% identified as the most effective doping level for enhancing the photocatalytic performance of $SrTiO_3$. Besides, these results confirm the important role of Pr in tailoring $SrTiO_3$ defects and highlight coprecipitation as an effective and environmentally friendly synthesis route for sustainable photocatalysts in textile wastewater treatment. Finally, for the practical implication, these findings demonstrated that Pr-doped $SrTiO_3$ is a promising material that can be optimized for industrial wastewater treatment systems.

The combination of scalability, structural stability, and moderate photocatalytic enhancement makes it an attractive candidate for future research aimed at sustainable and economically viable solar-powered water purification strategies.

ACKNOWLEDGEMENT

The authors thank Universitas Sebelas Maret for supporting this research through the Rencana Kerja dan Anggaran Tahunan (RKAT or Annual Work Plan and Budget) of Universitas Sebelas Maret in 2025, specifically through the Penguatan Kapasitas Grup Riset (PKGR-UNS or Strengthening the Capacity of Research Groups) project, with contract number 371/UN27.22/PT.01.03/2025.

REFERENCES

[1] I. Jerin, M. A. Rahman, A. H. Khan, and M. M. Hossain. "Photocatalytic Degradation of Methylene Blue Under Visible Light Using Carbon-Doped Titanium Dioxide as Photocatalyst." *Desalination and Water Treatment,* vol. 320, 2024.

[2] A. Syoufian and R. Kurniawan. "Visible-Light-Induced Photodegradation of Methylene Blue Using Mn,N-codoped $ZrTiO_4$ as Photocatalyst." *Indonesian Journal of Chemistry,* vol. 23, no. 3, 2023.

[3] N. P. Rini, N. I. Istiqomah, Sunarta, and E. Suharyadi. "Enhancing Photodegradation of Methylene Blue and Reusability Using CoO/ZnO Composite Nanoparticles." *Case Studies in Chemical and Environmental Engineering,* vol. 7, 2023.

[4] H. Shukla, R. Gautam, Sushma, and N. Kumari. "A Comprehensive Review: Photodegradation of Dyes with Rare Earth Doped Metal Oxide Nanoparticles for Wastewater Treatment." *Journal of Physics and Chemistry of Solids,* vol. 200, 2025.

[5] S. Khan, T. Noor, N. Iqbal, and L. Yaqoob. "Photocatalytic Dye Degradation from Textile Wastewater: A Review." *ACS Omega,* vol. 9, no. 20, pp. 21751–21767, 2024.

[6] S. Mehra, J. Saroha, E. Rani, V. Sharma, L. Goswami, G. Gupta, A. K. Srivastava, and S. N. Sharma. "Development of Visible Light-Driven $SrTiO_3$ Photocatalysts for the Degradation of Organic Pollutants for Waste-Water Treatment: Contrasting Behavior of MB & MO Dyes." *Optical Materials,* vol. 136, 2023.

[7] P. C. Paul, D. K. Mahato, and M. Mahato. "Fe-doped $SrTiO_3$ perovskites: Exploring Their Applications in Photocatalytic Dye Degradation and Supercapacitors." *Frontiers of Materials Science,* vol. 19, no. 2, 2025.

[8] U. Abdikarimova, M. Bissenova, N. Matsko, A. Issadykov, I. Khromushin, T. Aksenova, K. Munasbayeva, E. Slyamzhanov, and A. Serik. "Visible Light-Driven Photocatalysis of Al-Doped $SrTiO_{(3)}$: Experimental and DFT Study," *Molecules,* vol. 29, no. 22, p. 5326.

[9] Y. Iriani, R. Afriani, D. K. Sandi, and F. Nurosyid. "Co-precipitation Synthesis and Photocatalytic Activity of Mndoped $SrTiO_3$ for the Degradation of Methylene Blue Wastewater." *EVERGREEN Joint Journal of Novel Carbon Resource Sciences & Green Asia Strategy,* vol. 09, no. 04, pp. 1039–1045, 2022.

[10] I. Qadir, S. Singh, S. Sharma, U. Manhas, A. K. Atri, and D. Singh. "New Rare Earth-Doped Bilayered Perovskite Oxide Photocatalysts $Sr_{(2)}La_{(0.5)}R_{(0.5)}FeMnO_{(7)}$ (R = La, Nd, Sm, Gd, Dy) for the Degradation of Highly Toxic Methylene Blue Dye in Wastewater under Visible Light: Structural, Optical, and Magnetic Properties." *ACS Omega,* vol. 8, no. 2, pp. 2010–2026, 2023.

[11] Y. Wang, W. Ma, Y. Song, J. Chen, J. Xu, D. Wang, and Z. Mao. "Enhanced Photocatalytic Performance of $SrTiO_3$ Powder Induced by Europium Dopants." *Journal of Rare Earths,* vol. 39, no. 5, pp. 541–547, 2021.

[12] Y.-X. Song, W.-Q. Ma, J.-J. Chen, J. Xu, Z.-Y. Mao, and D.-J. Wang. "Photocatalytic Activity of Perovskite $SrTiO_3$ Catalysts Doped with Variable Rare Earth Ions." *Rare Metals,* vol. 40, no. 5, pp. 1077–1085, 2021.

[13] Q. Zhang, C. Li, Z. Li, N. Wang, X. Chen, C. Zhang, J. Xing, H. Qi, and Q. Xing. "Enhanced Degradation of Methylene Blue by Three-Dimensional Ordered Ceria and Strontium Titanate Composite Heterojunction Visible Photocatalyst Activated Peroxymonosulfate." *Journal of Materials Science,* vol. 59, no. 5, pp. 1877–1895, 2024.

[14] D. Doğu and K. Gürkan. "Praseodymium katkılı titanyum dioksit fotokatalizörünün metilen mavisinin bozunma reaksiyonundaki etkinliği." *Gazi Üniversitesi Mühendislik Mimarlık Fakültesi Dergisi,* vol. 35, no. 2, pp. 859–870, 2019.

[15] T. L. Soundarya, R. Harini, K. Manjunath, Udayabhanu, B. Nirmala, and G. Nagaraju. "Pt-doped TiO_2 Nanotubes as Photocatalysts and Electrocatalysts for Enhanced Photocatalytic H_2 Generation, Electrochemical Sensing, and Supercapacitor Applications." *International Journal of Hydrogen Energy,* vol. 48, no. 82, pp. 31855–31874, 2023.

[16] A. Mancuso, O. Sacco, V. Vaiano, D. Sannino, S. Pragliola, V. Venditto, and N. Morante. "Visible Light Active Fe-Pr co-doped TiO_2 for Water Pollutants Degradation." *Catalysis Today,* vol. 380, pp. 93–104, 2021.

[17] I. Ahmad, M. S. Akhtar, E. Ahmed, and M. Ahmad. "Facile Synthesis of Pr-Doped ZnO Photocatalyst Using Sol–Gel Method and Its Visible Light Photocatalytic Activity." *Journal of Materials Science: Materials in Electronics,* vol. 31, no. 2, pp. 1084–1093, 2019.

[18] S. Choudhary and S. Mohapatra. "Efficient Photocatalytic Degradation of Antibiotic Levofloxacin and Organic Pollutants in Water by Pr Doped ZnO Nanorods." *Chemical Physics Impact,* vol. 9, 2024.

[19] Y. Iriani, N. F. S. Puspita, D. K. Sandi, F. Nurosyid, R. Suryana, and D. Fasquelle. "The Improved Photocatalytic Performance of Strontium Titanate (STO) Powder Induced by Lanthanum Dopants." *Iranian Journal of Materials Science and Engineering,* vol. 21, no. 4, pp. 1–10, 2023.

[20] E. Zhou, J.-M. Raulot, H. Xu, H. Hao, Z. Shen, and H. Liu. "Structural, Electronic, and Optical Properties of Rare-Earth-Doped $SrTiO_3$ Perovskite: A First-Principles Study." *Physica B: Condensed Matter,* vol. 643, 2022.

[21] M. Shah, P. K. J. Sanam, and P. P. Pradyumnan. "Tuning of Photoluminescence Properties: Impact of Pr-doping in $SrTiO_3$ Crystallites." *Materials Today Communications,* vol. 39, 2024.

[22] M. Plonska and J. Plewa. "Investigation of Praseodymium Ions Dopant on 9/65/35 PLZT Ceramics' Behaviors, Prepared by the Gel-Combustion Route." *Materials (Basel),* vol. 16, no. 23, 2023.

[23] D. Kim, S. Gwon, K. Park, and E.-C. Jeon. "Structural and Optical Properties of $SrTiO_3$-Based Ceramics for Energy and Electronics Applications." *Crystals,* vol. 14, no. 11, 2024.

[24] M. M. Ravindra, R. Shirasangi, H. P. Dasari, and M. B. Saidutta. "Fabrication of Praseodymium-Doped Ceria (PDC) Films by Slurry Spin-Coating Technique and Its Structural, Morphological and Optical Properties." *Applied Surface Science Advances,* vol. 16, 2023.

[25] M. L. Ghimire, D. L. Kunwar, J. N. Dahal, D. Neupane, S. Yoon, and S. R. Mishra. "Co-Doped Rare-Earth (La, Pr) and Co-Al Substituted M-Type Strontium Hexaferrite: Structural, Magnetic, and Mossbauer Spectroscopy Study." *Materials Sciences and Applications,* vol. 11, no. 07, pp. 474–493, 2020.

[26] J. S. Punitha, R. K. Raji, T. Ramachandran, K. S. Kumar, M. Dhilip, F. Hamed, and A. Nataraj. "Influence of Pr^{3+} Substitution on The Structural, Optical, Magnetic, and Dielectric Properties of $Sr_2FeTiO_{6-\delta}$ Double Perovskites." *Solid State Sciences,* vol. 160, p. 107825, 2025.

[27] Y. Xu, P. Wu, M. Wu, Y. Gu, H. Yu, and Z. Ding. "Solvothermal Synthesis, Structural Characterization and Optical Properties of Pr-Doped $CeO_{(2)}$ and Their Degradation for Acid Orange 7." *Materials (Basel),* vol. 15, no. 19, 2022.

[28] K. N. Clayton, J. W. Salameh, S. T. Wereley, and T. L. Kinzer-Ursem. "Physical Characterization of Nanoparticle Size and Surface Modification using Particle Scattering Diffusometry." *Biomicrofluidics,* vol. 10, no. 5, p. 054107.

[29] J. Jeevanandam, M. Goncalves, R. Castro, J. Gallo, M. Banobre-Lopez, and J. Rodrigues. "Stabilization of Metal-Doped Magnesium Oxide Nanoparticles with PAMAM Dendrimers to Improve Alpha-Amylase Enzyme Inhibition." *Mater Today Bio,* vol. 31, p. 101520, 2025.

[30] A. Zindrou, P. Psathas, and Y. Deligiannakis. "Flame Spray Pyrolysis Synthesis of Vo-Rich Nano-$SrTiO_{(3-x)}$." *Nanomaterials (Basel),* vol. 14, no. 4, 2024.

[31] I. A. Sluchinskaya, A. I. Lebedev, and A. Erko. "Crystal structure, local structure, and defect structure of Pr-doped $SrTiO_3$." *Journal of Applied Physics,* vol. 112, no. 2, 2012.

[32] A. Jraba, J. Soli, L. El Mir, and E. Elaloui. "Improvement of Properties and Catalytic Activity of TiO_2 for the Adsorption and Solar Photodecomposition of Ibuprofen: Effect of Er^{3+} and Pr^{3+} Doping." *Journal of Materials Science: Materials in Electronics,* vol. 33, no. 18, pp. 15005–15022, 2022.

[33] D. K. Bhat, U. Pi, and U. S. Shenoy. "Insights Into the Dopant Engineering in Copper-Doped $SrTiO_3$ Nanocubes." *Journal of Hazardous Materials Advances,* vol. 12, 2023.

[34] A. M. Dehkordi, S. Bhattacharya, T. Darroudi, H. N. Alshareef, and T. M. Tritt. "New Insights on the Synthesis and Electronic Transport in Bulk Polycrystalline Pr-doped $SrTiO_{3-\delta}$." *Journal of Applied Physics,* vol. 117, no. 5, 2015.

[35] M. Shah, S. P. K. Jamshina, and P. P. Pradyumnan. "Optimization of Carrier Mobility in Pr-doped $SrTiO_3$ Thin Films through Controlled Sr-Segregation for Optoelectronic Applications." *Surfaces and Interfaces,* vol. 55, 2024.

[36] C. Zhang, N. Jiang, S. Xu, Z. Li, X. Liu, T. Cheng, A. Han, H. Lv, W. Sun, and Y. Hou. "Towards High Visible Light Photocatalytic Activity in Rare Earth and N co-doped $SrTiO_3$: A First Principles Evaluation and Prediction." *RSC Advances,* vol. 7, no. 27, pp. 16282–16289, 2017.

[37] W. Wang, C. Jiang, M. Shen, L. Fang, F. Zheng, X. Wu, and J. Shen. "Effect of Oxygen Vacancies on the Red Emission of $SrTiO_3$:Pr^{3+} Phosphor Films." *Applied Physics Letters,* vol. 94, no. 8, 2009.

[38] X. Ran, "Y. Bai, H. Zeng, J. Zhang, H. Fu, X. An, and X. Yang. "Manipulating Oxygen Vacancy in $SrTiO_3$ Nanoparticles to Achieve Enhanced Photoelectrochemical Performance in Water Splitting." *ACS Applied Nano Materials,* vol. 7, no. 23, pp. 27543–27554, 2024.

[39] M. RaeisianAsl, S. Jouybar, S. Sarabadani Tafreshi, and L. Naji. "Exploring the Key Features for Enhanced $SrTiO_3$ Functionality: A Comprehensive Overview." *Materials Today Sustainability,* vol. 29, 2025.

[40] R. Garg, A. Senyshyn, H. Boysen, and R. Ranjan. "Structure of the Noncubic Phase in the Ferroelectric State of Pr-Substituted $SrTiO_3$." *Physical Review B,* vol. 79, no. 14, 2009.

[41] A. Mehdizadeh Dehkordi, S. Bhattacharya, T. Darroudi, X. Zeng, H. N. Alshareef, and T. M. Tritt. "Synthesis of Non-Uniformly Pr-doped $SrTiO_3$ Ceramics and Their Thermoelectric Properties." *J Vis Exp,* no. 102, p. e52869, 2015.

[42] M. Kudus, A. J. Kostić, M. M. Savanović, S. J. Armaković. "Comparison of photocatalytic performance of $Sr_{0.9}$ $La_{0.1}TiO_3$ and $Sr_{0.25}Ca_{0.25}Na_{0.25}Pr_{0.25}TiO_3$ toward metoprolol and pindolol photodegradation." *Metallurgical and Materials Data,* vol. 1, no. 1, 2023.

[43] S. S. Mohtar, F. Aziz, A. F. Ismail, N. S. Sambudi, H. Abdullah, A. N. Rosli, and B. Ohtani. "Impact of Doping and Additive Applications on Photocatalyst Textural Properties in Removing Organic Pollutants: A Review." *Catalysts,* vol. 11, no. 10, 2021.

[44] P.-S. Konstas, I. Konstantinou, D. Petrakis, and T. Albanis. "Development of $SrTiO_3$ Photocatalysts with Visible Light Response Using Amino Acids as Dopant Sources for the Degradation of Organic Pollutants in Aqueous Systems." *Catalysts,* vol. 8, no. 11, 2018.

[45] Y. Ham, T. Hisatomi, Y. Goto, Y. Moriya, Y. Sakata, A. Yamakata, J. Kubota, and K. Domen. "Flux-Mediated Doping of $SrTiO_3$ Photocatalysts for Efficient Overall Water Splitting." *Journal of Materials Chemistry A,* vol. 4, no. 8, pp. 3027–3033, 2016.

[46] T. Xie, Y. Wang, C. Liu, and L. Xu. "New Insights into Sensitization Mechanism of the Doped Ce (IV) into Strontium Titanate." *Materials (Basel),* vol. 11, no. 4, 2018.

[47] Y. Xu, Y. Liang, Q. He, R. Xu, D. Chen, X. Xu, and H. Hu. "Review of Doping $SrTiO_3$ for Photocatalytic Applications." *Bulletin of Materials Science,* vol. 46, no. 1, 2022.

[48] A. Jovanoski Kostic *et al.*, "Evaluation of Photocatalytic Performance of Nano-Sized $Sr_{(0.9)}La_{(0.1)}TiO_{(3)}$ and $Sr_{(0.25)}Ca_{(0.25)}Na_{(0.25)}Pr_{(0.25)}TiO_{(3)}$ Ceramic Powders for Water Purification" *Nanomaterials (Basel),* vol. 12, no. 23, Nov 25 2022. doi: 10.3390/nano12234193 Available: https://www.ncbi.nlm.nih.gov/pubmed/36500815

[49] S. M. Tichapondwa, J. P. Newman, and O. Kubheka. "Effect of TiO_2 Phase on the Photocatalytic Degradation of Methylene Blue Dye." *Physics and Chemistry of the Earth, Parts A/B/C,* vol. 118–119, 2020.

[50] B. Boga, N. Steinfeldt, N. G. Moustakas, T. Peppel, H. Lund, J. Rabeah, Z. Pap, V.-M. Cristea, and J. Strunk. "Role of $SrCO_3$ on Photocatalytic Performance of $SrTiO_3$-$SrCO_3$ Composites." *Catalysts,* vol. 12, no. 9, 2022.
[51] X. Pan, X. Chen, and Z. Yi. "Photocatalytic Oxidation of Methane Over $SrCO_3$ decorated $SrTiO_3$ Nanocatalysts via a Synergistic Effect." *Phys. Chem. Chem. Phys.,* vol. 18, no. 46, pp. 31400–31409, 2016.